

# Results from an extended Falcon all-sky survey for continuous gravitational waves

Vladimir Dergachev<sup>1,2, a</sup> and Maria Alessandra Papa<sup>1,2,3, b</sup>

<sup>1</sup>*Max Planck Institute for Gravitational Physics (Albert Einstein Institute), Callinstrasse 38, 30167 Hannover, Germany*

<sup>2</sup>*Leibniz Universität Hannover, D-30167 Hannover, Germany*

<sup>3</sup>*University of Wisconsin Milwaukee, 3135 N Maryland Ave, Milwaukee, WI 53211, USA*

We present the results of an all-sky search for continuous gravitational wave signals with frequencies in the 200-600 Hz range and frequency derivative (spindown) from  $-1 \times 10^{-8}$  through  $1.11 \times 10^{-9}$  Hz/s. Together with the results from [1], this search completes the all-sky survey for frequencies between 20 to 600 Hz on O1 data. It also demonstrates the scalability of our search on a parameter space 26 times larger than previously considered. The results presented here complement the LIGO O2 data results [2, 3] with comparable when not better sensitivity and do not rely on data with irregularities in the noise-subtraction procedure. We establish strict upper limits which hold for worst-case signal parameters and dedicated upper limits for generic  $\approx 0$  spindown signals, such as those expected from boson condensates around black holes.

Broad-band all-sky searches for continuous gravitational waves are computationally challenging. The most sensitive searches rely on clever search methods, computationally efficient algorithms and much computing power [1, 4–7].

The loosely coherent approach that we have adopted for our broadest and fast-turnaround surveys has proven to be very successful with short coherence time lengths ( $\approx$  half an hour) [8–10]. Its recent extension to longer coherent timescales, the Falcon search, represents a breakthrough in performance and sensitivity [1].

The first Falcon search [1] demonstrates the new method investigating the frequency range 20-200 Hz, all-sky, on data from LIGO’s first observation run (O1) [11–13]. Here we extend the search to the frequency region 200-600 Hz. The frequency derivative in both searches is from  $-1 \times 10^{-8}$  through  $1.11 \times 10^{-9}$  Hz/s. The same five-stage pipeline is used, starting with coherence length of 4 hours.

Even with the most efficient search strategies, continuous wave searches take a much longer time to complete than searches for transient signals and this time significantly grows with increasing signal frequency. In particular, since the number of sky templates scales quadratically with frequency, the size of the parameter space of this search is 26 times greater than that of [1]. As a consequence it took a longer time to carry out this search, in comparison with [1]. We use O1 data because this search was started before the O2 data [14] had been made public. This search demonstrates that the efficiency of Falcon is maintained in a significantly larger production run.

The full list of outliers that survive all the stages is available in [15]. Table I shows a summary of this list. The summary excludes all outliers within 0.01 Hz of multiples of 0.5 Hz, which are induced by 0.25 Hz combs of instrumental lines [16]. The remaining outliers are summarized by displaying the largest SNR outlier in every

0.1 Hz band. The top 7 outliers are caused by hardware injected simulated signals whose parameters are listed in Table II. The large majority are due to large hardware artifacts. A few dozen outliers cannot be ascribed to instrumental causes based on  $h(t)$  data alone. Studies based on physical and environmental monitoring channels, that are not public, could shed more light on their origin.

We compute 95% confidence level upper limits on the intrinsic gravitational wave amplitude  $h_0$  of a quasi-monochromatic signal with slow evolution in frequency that can be approximated by a linear model. These are shown in Figure 1. The upper limit data is available in computer-readable format in [15]. We also provide upper limits for  $\approx 0$  spindown signals, relevant for boson condensates around black holes [17, 18]. We leave it to the interested reader to constrain from our upper limits physical quantities of interest, based on the specific model they wish to consider.

The upper limits are computed using the universal statistic algorithm [19] and are valid in all frequency bands and for the entire sky. The worst case and circular polarization 95% confidence level upper limits are obtained by maximizing upper limits established for individual sky locations, spindowns and frequency bands. Therefore, they are applicable to any subset of the searched parameter space. The population-average proxy upper limits are provided for ease of comparison with other search results [2, 4, 16, 20]. They are computed as weighted average of upper limits from individual polarizations. We use the same weighting as in [1].

Figure 2 presents circular polarization upper limits converted into maximum distance curves [16, 20]. At the high end of the frequency range we are sensitive to a source with  $10^{-6}$  equatorial ellipticity up to 2.7 kpc away. It is known that neutron stars can readily support equatorial ellipticities of more than  $10^{-6}$  [21, 22].

Compared to the O2 data-set, the O1 data-set is less sensitive in many frequency bands, has larger instrumental contamination and half the accumulated time. Nevertheless, the upper limits presented here are comparable to the LIGO-Virgo collaboration results [3] and to [2] on

<sup>a</sup> vladimir.dergachev@aei.mpg.de

<sup>b</sup> maria.alessandra.papa@aei.mpg.de

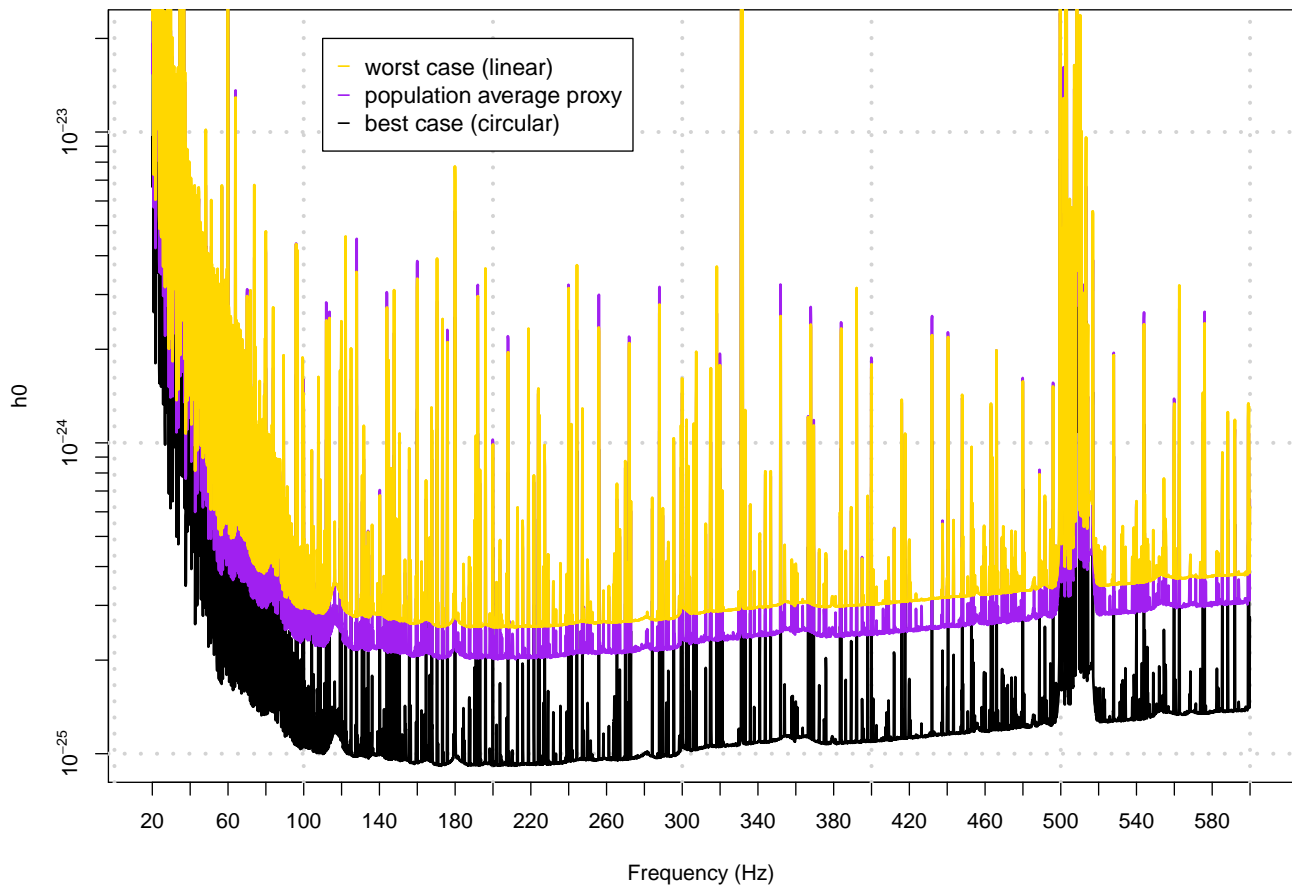


FIG. 1. O1 upper limits. The dimensionless strain (vertical axis) is plotted against signal frequency. Looking at the right side of the plot, the upper (yellow) curve shows worst-case upper limits, the next lower curve (purple) shows the population average proxy, followed by the black curve showing best-case upper limits (circularly polarized signals). The worst-case and best-case upper limits are maximized over sky and all intrinsic signal parameters for each frequency band displayed. For completeness we include Falcon results in the frequency range 20-200 Hz from [1].

O2 data. In the 500-600 Hz frequency range our upper limits are more constraining than those of [2, 3].

The O2 data used in [2, 3] was subject to a cleaning procedure that removed substantial amount of spurious instrumental noise. The cleaning procedure was originally designed for short-lived signals [23] but was subsequently applied to the entire data stream.

The basic idea of the cleaning procedure is to fit  $h(t)$  data to many witness data streams and to subtract the polluting contributions. This requires the transfer function from witness data to  $h(t)$  to be estimated. The transfer function is non stationary and the estimation is performed in-sample separately on a high number of short time intervals – and correspondingly small amounts of data. Accidental correlations, which are more likely to happen when the fits are done using small data-sets, can lead to “over-cleaning”, an example of which are the

spikes below the noise floor level in Figure 1 of [3]. In general this procedure will contribute an additional systematic uncertainty to the calibration. Whereas we have no reason to believe that such uncertainty amounts to more than a few percent, it is not discussed in [3]<sup>1</sup>. Our results provide strict upper limits at a comparable level of sensitivity, derived from a data-set not treated with such procedure.

We also note the interesting discussion of signals from ultra-light bosons in [2]. The population average upper limits in [2] are derived from a signal population that is

<sup>1</sup> Public O2 data is limited to the cleaned  $h(t)$  data. The release of the uncleaned  $h(t)$  and the witness channels would allow for an independent assessment of the extent of this effect.

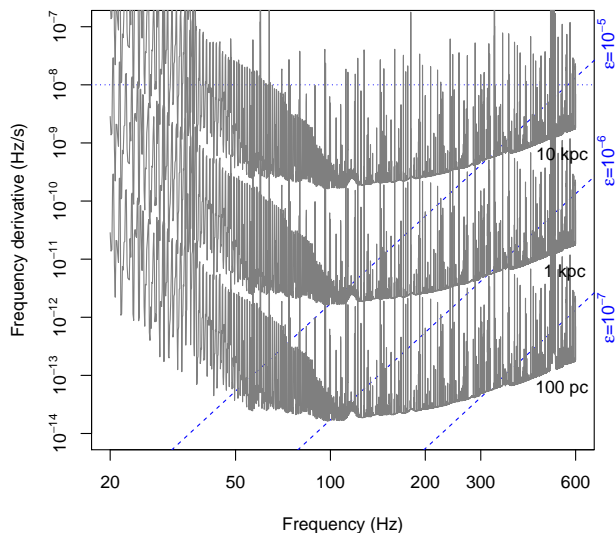


FIG. 2. Range of the search for neutron stars spinning down solely due to gravitational radiation. This is a superposition of two contour plots. The grey solid lines are contours of the maximum distance at which a neutron star could be detected as a function of gravitational wave frequency  $f$  and its derivative  $\dot{f}$ . The dashed lines are contours of the corresponding ellipticity  $\epsilon(f, \dot{f})$ . The fine dotted line marks the maximum spindown searched. Together these quantities tell us the maximum range of the search in terms of various populations [16, 20]

*much* larger than that of boson signals. It is not immediately clear to us how to translate a population-average upper limit into an upper limit for a very tiny subset of that population. We use instead a strict worst-case upper limit from the  $\approx 0$  spindown search results *only*.

In conclusion, we have applied the Falcon pipeline to O1 open data. We explore frequencies from 20 to 600 Hz and frequency derivative from  $-1 \times 10^{-8}$  through  $1.11 \times 10^{-9}$  Hz/s, not relying on data with irregularities in the noise-subtraction procedure. We establish strict upper limits over the entire spindown range and provide dedicated upper limits for generic  $\approx 0$  spindown signals, such as those expected from boson condensates around black holes.

The search was performed on the ATLAS cluster at AEI Hannover. We thank Bruce Allen, Carsten Aulbert and Henning Fehrmann for their support. We also thank Heinz-Bernd Eggenstein and Badri Krishnan for helpful comments and suggestions.

This research has made use of data, software and/or web tools obtained from the LIGO Open Science Center (<https://losc.ligo.org>), a service of LIGO Laboratory, the LIGO Scientific Collaboration and the Virgo Collaboration. LIGO is funded by the U.S. National Science Foundation. Virgo is funded by the French Centre

National de Recherche Scientifique (CNRS), the Italian Istituto Nazionale della Fisica Nucleare (INFN) and the Dutch Nikhef, with contributions by Polish and Hungarian institutes.

Idx	SNR	Frequency Hz	Spindown nHz/s	RA <sub>J2000</sub> degrees	DEC <sub>J2000</sub> degrees	Description
1	990	575.16353	-0.002	215.266	3.420	Hardware injection ip2
2	870	52.80832	0.006	306.634	-83.997	Hardware injection ip5
3	637	191.03126	-8.652	351.425	-33.552	Hardware injection ip8
5	577	265.57554	-0.006	71.522	-56.250	Hardware injection ip0
6	387	146.16934	-6.710	359.608	-65.199	Hardware injection ip6
7	376	38.47793	-6.235	332.323	-14.679	Hardware injection ip12
9	300	108.85718	-0.006	178.641	-33.400	Hardware injection ip3
21	76	440.01500	-3.465	64.741	-89.269	Coincident bin-centered lines in H1 and L1 at 440 Hz
27	54	99.97667	-5.115	100.314	-41.321	coincident contamination in LHO and LLO
28	50	31.51238	-5.619	226.702	-23.180	Heavy contamination, 0.25 Hz comb in H1, 31.512 Hz line in L1
35	39	568.01983	-4.590	10.582	-89.728	Coincident bin-centered lines at 568 Hz in H1 and L1
40	27	65.51035	-5.419	198.120	-40.763	0.25 Hz comb of instrumental lines
43	25	460.31067	-6.248	248.229	25.004	Bin-centered line in L1 at 460.3 Hz
44	24	213.01333	-5.794	200.927	-76.281	Strong bin-centered line in L1 at 213 Hz
45	24	346.79879	-9.548	118.917	-66.016	Strong bin-centered line in L1 at 346.8 Hz
46	23	499.28421	-3.294	113.162	-85.284	
47	23	32.69785	-9.940	45.757	-37.300	Lack of coherence, contamination in H1
48	23	336.03237	-9.206	46.881	-64.585	Strong bin-centered line in H1 at 336 Hz
49	23	489.40904	-0.619	105.644	-87.021	
51	21	82.51584	-3.994	157.388	-46.681	Lack of coherence, 0.25 Hz comb in H1
52	21	81.52983	-6.310	332.731	-45.648	0.25 Hz comb of instrumental lines
53	21	400.91107	-7.790	236.031	-14.678	Bin-centered line in L1 at 400.9 Hz
54	21	107.13643	-6.677	12.094	-57.316	coincident artifacts at 107.12 Hz in H1 and L1
55	21	395.10804	-7.269	235.216	-2.870	Strong bin-centered line in L1 at 395.1 Hz
56	21	504.04105	-8.631	45.942	-34.696	Contaminated spectrum in L1
57	21	494.64592	-1.252	290.051	-6.967	Bin-centered line in L1 at 494.6 Hz
58	21	575.21330	-5.623	244.809	-26.514	Induced by injected pulsar 2
59	20	389.25710	-4.085	133.784	8.790	Strong bin-centered line in L1 at 389.3 Hz
61	20	450.97950	-2.673	138.341	-71.593	Large broad line in H1
63	20	113.01128	1.044	304.688	9.253	0.25 Hz comb of instrumental lines
66	19	90.65642	-6.944	302.827	59.828	no coherence, disturbed H1 spectrum
67	19	542.80440	-2.160	225.365	73.334	
69	19	372.38427	-7.227	194.433	-5.782	Strong bin-centered line in L1 at 372.4 Hz
70	19	263.70538	-6.265	267.151	-6.564	Spectrum disturbance in L1 at 263.68 Hz
71	19	232.01442	-4.702	253.569	-32.984	Strong bin-centered line in H1 at 232 Hz
72	19	62.80672	-7.985	276.491	-12.515	Sharp bin-centered line in L1 at 62.8 Hz
73	19	45.01809	-1.227	186.589	28.604	Lines in H1 and L1 at 45 Hz, contaminated spectrum
74	19	558.82419	-3.890	96.652	-42.306	
75	19	523.31879	-4.381	62.264	-29.181	
76	19	507.88723	-9.340	215.354	-22.646	Disturbed spectrum in H1, L1, artifact in H1
77	19	500.47631	-3.069	223.181	22.283	Disturbed spectrum
78	18	329.90057	-5.369	209.627	-43.310	Strong bin-centered line in L1 at 329.9 Hz
79	18	595.69484	-7.548	135.507	-40.958	
80	18	133.30755	-6.548	124.281	-50.348	Line in L1 at 133.33 Hz
81	18	431.80112	-2.415	139.466	-73.854	Bin-centered line in L1 at 431.8 Hz
82	18	49.96416	-9.906	335.191	-18.085	Highly contaminated spectrum
83	18	437.51154	-8.248	34.774	-81.896	
84	18	389.32134	-9.310	240.622	-40.377	Strong bin-centered line in L1 at 389.3 Hz
85	18	494.79751	-3.385	51.134	-85.496	Weak peak in H1
86	18	164.68348	-4.927	48.010	-9.672	Line in L1 at 164.7 Hz
87	18	265.60671	-6.777	55.182	-46.651	Induced by injected pulsar 0
88	18	86.51503	-5.252	56.836	-36.012	Coincident lines at 86.5 Hz, 0.25 Hz comb, sloping spectrum in L1
89	18	289.83178	-7.869	82.058	-42.351	Strong bin-centered line in L1 at 289.8 Hz
90	18	48.98773	-4.410	43.189	-22.949	Highly contaminated H1 and L1 spectrum near 49 Hz
91	18	437.47776	0.556	243.755	77.132	Sharp line in H1
92	18	493.92431	-5.498	54.876	-81.477	
93	18	586.05732	-8.790	106.536	56.297	
94	18	437.16341	-2.285	46.974	-55.430	
95	18	474.80102	0.452	82.433	-66.225	Bin-centered line in L1 at 474.8 Hz
96	18	192.83187	-7.790	248.222	46.044	Contaminated H1 spectrum
97	18	520.38580	-8.852	199.175	-17.384	Broad peak in H1
98	18	505.25220	-8.515	217.942	-6.080	Disturbed spectrum
99	18	583.20390	-3.969	264.475	19.116	
101	18	536.07116	0.860	340.569	32.085	
102	18	313.91131	-2.856	279.757	-19.852	
104	18	263.30291	0.552	248.540	-12.794	
105	18	292.73093	-8.140	91.585	-71.773	Strong bin-centered line in L1 at 292.7 Hz
107	18	54.12124	-9.790	225.480	-16.962	Sharp bin-centered line in L1 at 54.1 Hz
108	17	402.62921	-9.381	78.985	-29.987	
109	17	403.69274	-5.406	267.397	49.040	
110	17	576.71810	-0.994	149.248	-87.368	Bin-centered line in L1 at 576.7 Hz
111	17	520.16849	-5.810	139.840	-38.511	Bin-centered line in L1 at 520.2 Hz
112	17	307.06911	-3.319	37.475	-36.676	
114	17	235.71326	-5.585	248.190	-9.510	Strong bin-centered line in L1 at 235.7 Hz
115	17	573.81279	-8.410	245.184	20.706	Bin-centered line in L1 at 573.8 Hz
116	17	360.81832	-7.048	248.604	-26.722	Strong bin-centered line in L1 at 360.8 Hz
117	17	569.11624	-2.552	101.200	-31.105	
118	17	499.18839	-5.898	112.912	-4.852	
119	17	264.88175	-7.019	128.380	30.645	
120	17	545.75305	-8.185	148.278	-17.831	Bin-centered line in L1 at 545.8 Hz
121	17	476.19888	0.706	187.584	76.698	
122	17	527.75761	-7.119	42.136	-87.901	
123	17	583.70009	-4.719	279.324	21.711	
124	17	496.30591	1.094	70.496	-62.031	
125	17	594.72548	-5.665	191.759	-57.949	
126	17	91.71446	-8.506	128.301	-28.413	Disturbed spectrum in H1 and L1
127	17	233.30599	-3.310	248.211	21.634	Strong bin-centered line in L1 at 233.3 Hz
128	17	383.51603	-8.977	238.020	-20.427	Strong bin-centered line in L1 at 383.5 Hz
129	17	519.40183	-3.510	297.494	-4.499	
130	17	338.13859	-1.535	354.725	-18.423	Strong bin-centered line in H1 at 338.1 Hz
131	17	572.25638	-5.327	103.114	-29.292	
132	17	550.96513	-7.510	177.002	41.547	
133	17	371.20547	-10.065	80.438	40.981	
134	17	489.90223	0.727	243.597	41.975	
135	17	249.69852	1.056	299.094	75.656	Strong bin-centered line in L1 at 249.7 Hz, near ecliptic pole
136	17	489.75017	-2.048	223.733	52.532	
137	17	363.36911	-1.706	223.220	-25.441	
139	17	457.94864	-7.819	170.523	54.718	
140	17	409.12979	-3.598	294.263	31.772	Bin-centered line in L1 at 409.1
141	17	340.16488	-1.373	21.686	33.143	
142	17	365.08911	0.356	268.928	32.316	
143	17	53.93050	-2.956	212.788	-24.064	Disturbed H1 spectrum
144	17	595.42453	-6.160	105.539	-39.152	
145	17	498.90070	0.860	254.355	31.267	
146	17	107.66022	-9.660	24.618	-6.139	Sharp line in L1 at 107.7 Hz
147	17	587.52000	-1.356	216.851	-53.248	
148	17	264.19402	-5.990	200.539	-21.531	Strong bin-centered line in L1 at 264.2 Hz
149	17	520.01878	-9.752	24.734	-38.491	
150	17	251.47765	-8.619	84.701	-25.529	
151	17	437.63312	-0.619	297.096	18.966	Bin-centered line in L1 at 437.6
152	17	335.05630	-7.027	110.027	-54.943	
153	17	517.76355	-4.727	177.760	42.038	Bin-centered line in L1 at 517.8 Hz

TABLE I. Outliers that passed the detection pipeline excluding outliers within 0.01 Hz of 0.25 Hz combs of instrumental lines. Only the highest-SNR outlier is shown for each 0.1 Hz frequency region. Outliers marked with “line” have strong narrowband disturbances near the outlier location. Signal frequencies refer to epoch GPS 1130529362. For completeness we include Falcon outliers in the frequency range 20-200 Hz from [1].

Label	Frequency Hz	Spindown nHz/s	RA <sub>J2000</sub> degrees	DEC <sub>J2000</sub> degrees
ip0	265.575533	$-4.15 \times 10^{-3}$	71.55193	-56.21749
ip2	575.163521	$-1.37 \times 10^{-4}$	215.25617	3.44399
ip3	108.857159	$-1.46 \times 10^{-8}$	178.37257	-33.4366
ip5	52.808324	$-4.03 \times 10^{-9}$	302.62664	-83.83914
ip6	146.169370	$-6.73 \times 10^0$	358.75095	-65.42262
ip8	191.031272	$-8.65 \times 10^0$	351.38958	-33.41852
ip10	26.341917	$-8.50 \times 10^{-2}$	221.55565	42.87730
ip11	31.424758	$-5.07 \times 10^{-4}$	285.09733	-58.27209
ip12	38.477939	$-6.25 \times 10^0$	331.85267	-16.97288

TABLE II. Parameters of the hardware-injected simulated continuous wave signals during the O1 data run (epoch GPS 1130529362). Because the interferometer configurations were largely frozen in a preliminary state after the first discovery of gravitational waves from a binary black hole merger, the hardware injections were not applied consistently. There were no injections in the H1 interferometer initially, and the initial injections in the L1 interferometer used an actuation method with significant inaccuracies at high frequencies.

- 
- [1] Sensitivity Improvements in the Search for Periodic Gravitational Waves Using O1 LIGO Data, Sensitivity Improvements in the Search for Periodic Gravitational Waves Using O1 LIGO Data, V. Dergachev and M. A. Papa, Phys. Rev. Lett. **123**, no. 10, 101101 (2019)
- [2] Direct constraints on ultra-light boson mass from searches for continuous gravitational waves, C. Palomba *et al.*, arXiv:1909.08854.
- [3] All-sky search for continuous gravitational waves from isolated neutron stars using Advanced LIGO O2 data, B. P. Abbott *et al.* (LIGO Scientific Collaboration and Virgo Collaboration), Phys. Rev. D **100** 024004 (2019).
- [4] First low-frequency Einstein@Home all-sky search for continuous gravitational waves in Advanced LIGO data, B. P. Abbott *et al.* (LIGO Scientific and Virgo Collaborations), Phys. Rev. D **96**, no. 12, 122004 (2017)
- [5] Optimizing the choice of analysis method for all-sky searches for continuous gravitational waves with Einstein@Home, S. Walsh, K. Wette, M. A. Papa and R. Prix, Phys. Rev. D **99**, no. 8, 082004 (2019)
- [6] Comparison of methods for the detection of gravitational waves from unknown neutron stars, S. Walsh *et al.*, Phys. Rev. D **94**, no. 12, 124010 (2016)
- [7] Fast and Accurate Sensitivity Estimation for Continuous-Gravitational-Wave Searches, C. Dreissigacker, R. Prix, K. Wette, Phys. Rev. D **98**, 084058 (2018)
- [8] On blind searches for noise dominated signals: a loosely coherent approach, V. Dergachev, Class. Quantum Grav. **27**, 205017 (2010).
- [9] Loosely coherent searches for sets of well-modeled signals, V. Dergachev, arXiv:1807.02351
- [10] Loosely coherent searches for medium scale coherence lengths, V. Dergachev, Phys. Rev. D **85**, 062003 (2012)
- [11] LIGO Open Science Center, <https://doi.org/10.7935/K57P8W9D>, (2018)
- [12] Advanced LIGO, J. Aasi *et al.* (LIGO Scientific Collaboration), Class. Quantum Grav. **32** 7 (2015)
- [13] M. Vallisneri *et al.* The LIGO Open Science Center, proceedings of the 10th LISA Symposium, University of Florida, Gainesville, May 18-23, 2014, arXiv:1410.4839
- [14] LIGO Open Science Center, <https://doi.org/10.7935/CA75-FM95>, (2019)
- [15] See EPAPS Document No. [number will be inserted by publisher] for numerical values of upper limits. Also at [www.aei.mpg.de/continuouswaves/01Falcon20\\_600](http://www.aei.mpg.de/continuouswaves/01Falcon20_600)
- [16] All-sky Search for Periodic Gravitational Waves in the O1 LIGO Data, B. P. Abbott *et al.* (LIGO Scientific Collaboration and Virgo Collaboration), Phys. Rev. D **96**, 062002 (2017)
- [17] Black Hole Superradiance Signatures of Ultralight Vectors, M. Baryakhtar, R. Lasenby, M. Teo, Phys. Rev. D **96**, 035006s
- [18] Black Hole Mergers and the QCD Axion at Advanced LIGO, A. Arvanitaki, M. Baryakhtar, R. Lasenby, S. Dimopoulos, S. Dubovsky, Phys. Rev. D **95**, 043001
- [19] A Novel Universal Statistic for Computing Upper Limits in Ill-behaved Background, V. Dergachev, Phys. Rev. D **87**, 062001 (2013).
- [20] Full Band All-sky Search for Periodic Gravitational Waves in the O1 LIGO Data, B. P. Abbott *et al.* (LIGO Scientific Collaboration and Virgo Collaboration), Phys. Rev. D **97** 102003 (2018).
- [21] Breaking Strain of Neutron Star Crust and Gravitational Waves, C. J. Horowitz and K. Kadau, Phys. Rev. Lett. **102**, 191102 (2009).
- [22] Maximum elastic deformations of relativistic stars, N. K. Johnson-McDaniel and B. J. Owen, Phys. Rev. D **88**, 044004 (2013)

- [23] J.C. Driggers *et al.* (LIGO Scientific Collaboration Instrument Science Authors), Improving astrophysical parameter estimation via offline noise subtraction for Advanced LIGO, Phys. Rev. D **99**, 042001 (2019).